

# Effects of nonlinear loss in high-Q Si ring resonators for narrow-linewidth III-V/Si heterogeneously integrated tunable lasers

CHAO XIANG,<sup>1,\*</sup>  WARREN JIN,<sup>1</sup>  JOEL GUO,<sup>1</sup>  COLEMAN WILLIAMS,<sup>1</sup>  ANDREW M. NETHERTON,<sup>1</sup>  LIN CHANG,<sup>1</sup>  PAUL A. MORTON,<sup>2</sup>  AND JOHN E. BOWERS<sup>1</sup> 

<sup>1</sup>*Department of Electrical and Computer Engineering, University of California, Santa Barbara, Santa Barbara, California 93106, USA*

<sup>2</sup>*Morton Photonics, West Friendship, Maryland 21794, USA*

\*[cxiang@ece.ucsb.edu](mailto:cxiang@ece.ucsb.edu)

**Abstract:** High-Q Si ring resonators play an important role in the development of widely tunable heterogeneously integrated lasers. However, while a high Q-factor ( $Q > 1$  million) is important for ring resonators in a laser cavity, the parasitic high-power density in a Si resonator can deteriorate the laser performance at high power levels due to nonlinear loss. Here, we experimentally show that this detrimental effect can happen at moderate power levels (a few milliwatts) where typical heterogeneously integrated lasers work. We further compare different ring resonators, including extended Si ring resonators and Si<sub>3</sub>N<sub>4</sub> ring resonators and provide practical approaches to minimize this effect. Our results provide explanations and guidelines for high-Q ring resonator designs in heterogeneously integrated tunable lasers, and they are also applicable for hybrid integrated butt-coupled lasers.

© 2020 Optical Society of America under the terms of the [OSA Open Access Publishing Agreement](#)

## 1. Introduction

The development of III-V/Si heterogeneously integrated lasers has entered a new era with rapidly growing needs in applications, such as optical interconnects [1], coherent optical communication [2] and LIDAR [3]. Among these applications, one important property of a high-performance laser source is the narrow laser linewidth, which can enable DSP-free high capacity data transmission and increase the optical sensing detection range and accuracy [4–5]. While typical monolithic III-V-based semiconductor lasers suffer from high spontaneous emission noise, heterogeneous integration of a silicon waveguide with III-V gain material provides access to phase noise control of semiconductor lasers [6]. To date, state-of-the-art heterogeneously integrated III-V/Si lasers exhibit laser linewidths several orders narrower (0.1~10 kHz) than monolithic III-V lasers (~MHz) [7–9].

Central to this improvement is the development of a laser cavity with an integrated low-loss Si waveguide. A low-loss Si waveguide can form a laser cavity with much higher quality factor (Q), i.e. increase the photon lifetime and thus leverage the laser coherence. A high-Q Si cavity with  $1.1 \times 10^6$  Q-factor is utilized to enable sub-kHz linewidth Si/III-V semiconductor laser [10]. Other than phase noise reduction of a solitary laser through mode engineering, external cavity lasers based on high-Q passive cavities provide another degree of freedom to further reduce the laser linewidth. Ultra-low loss Si waveguides with optical loss between 0.1 dB/cm to 1 dB/cm are a key enabler for recent reports of lasers with fundamental linewidth on the order of 100 Hz [9,11].

In many of these devices, high-Q Si ring resonators are used as an external cavity to provide narrow-band optical feedback and wide-band wavelength tuning. The performance metrics of a such a tunable laser largely rely on the design of cascaded ring resonators, including output power,

tuning range, and linewidth. However, when designing low-loss Si waveguides and high-Q rings for a high-performance tunable laser, most of the efforts were solely devoted to their passive performance without accounting for the parasitic limitations in a laser system. For example, a narrow linewidth laser favors high output power as its modified Schawlow-Townes linewidth scales with  $1/P$  [12]. At remarkably high-power levels, the performance of a Si ring resonator will differ from its own 'cold-cavity' performance at low-power levels, where its passive performance is normally characterized. While a high Q-factor improves photon lifetime and benefits laser coherence, it boosts the power level inside the ring resonator at the same time. This power build-up scales up with increased Q-factor for a ring resonator with fixed dimension [13,14]. However, Si has a relatively large two photon absorption (TPA) coefficient ( $\beta_{\text{TPA}} = 5 \times 10^{-12}$  m/W at  $1.55 \mu\text{m}$  [15]) and at high power levels, free carriers are generated, which results in free carrier absorption (FCA). So, at high power levels, the ring resonator Q-factor drops due to the increased nonlinear loss. While an important benefit of silicon photonic waveguides is its compact size, due to a high index-contrast with cladding material, its design needs to take the nonlinear loss into consideration, in addition to its cold-cavity performance.

The nonlinear loss in a high Q ring resonator has been widely studied including its impact on photon pair generation [16], effect on self-induced optical transmission modulation [17], and mitigation at cryogenic temperature operation [18] and in an integrated optical time magnifier [19].

The importance of reducing power density in ultra-low linewidth micro-ring resonator tunable laser designs was recognized by Morton *et al.*, [20,21], and led to the novel designs of 3 and 4 ring tunable lasers using low loss waveguides with large ring radii and lower Q rings. Low loss silicon nitride 3 and 4 ring laser reflectors were initially developed for these devices [22], which also avoided increased loss at higher power densities. Initial 3 and 4 ring ultra-low noise ultra-wideband tunable lasers using these designs, with low loss, large radii silicon waveguides, provided record linewidths and wavelength tuning [8,9]. These Si 'extended' ring resonators have large waveguide cross-sections and large ring radius. So together with low linear waveguide loss, the nonlinear loss will also be mitigated due to the decreased power intensity, benefiting the reported record narrow-linewidth laser performance.

In this paper, we experimentally characterized the power-dependent performance of high-Q ring resonators with different designs, including multimode Si ring resonators, quasi-single mode Si ring resonators, extended-radius Si ring resonators and  $\text{Si}_3\text{N}_4$  ring resonators. These ring resonators are fully compatible with current III-V/Si lasers and recently developed III-V/Si/ $\text{Si}_3\text{N}_4$  lasers [23]. Our results show that for high-Q Si resonators ( $Q > 1 \text{ M}$ , radius  $\sim 100 \mu\text{m}$ ), the nonlinear loss will start to dominate the total loss at a relatively low power level (a few milliwatts in the bus waveguide). Within this power range lies the typical output power of heterogeneously integrated III-V/Si lasers, which indicates the laser performance would be limited by nonlinear loss. As a comparison, the extended Si ring design could greatly reduce the impairment thanks to the reduced intracavity power build-up inside the ring resonator. Moreover, high-Q  $\text{Si}_3\text{N}_4$  ring resonators, which have negligible two photon absorption and free carrier generation, hold great potential in achieving a high-power heterogeneously integrated narrow-linewidth tunable laser. Our results provide an in-depth understanding of the effects of nonlinear loss in high-Q ring resonators, and a refined guidance for future design-of-choice of similar ring resonators in narrow linewidth heterogeneously integrated tunable lasers.

The paper is organized as follows – Section 2 discusses the nonlinear loss of high-Q Si ring resonators and the method for characterizing power dependent loss. Section 3 introduces the extended Si ring resonators and  $\text{Si}_3\text{N}_4$  ring resonators as two approaches to reduce or avoid nonlinear loss. Section 4 summarizes the nonlinear losses from different ring resonator designs and provides insight into heterogeneous laser performance with optimized nonlinear loss in ring resonators. Section 5 is a summary and outlook for future work.

## 2. High-Q Si ring resonators

We fabricate Si ring resonators on 100-mm-diameter silicon-on-insulator (SOI) wafers. The cross section of the fabricated ring resonator at the bus waveguide to ring waveguide coupling region is illustrated in Fig. 1(a). The buried SiO<sub>2</sub> layer is 1  $\mu\text{m}$  thick and the total thickness of the Si waveguide layer is 500 nm. The etch depth can be tailored to enable single mode and multimode waveguides, together with the choice of the Si width in the bus waveguide ( $W_{bus}$ ) and ( $W_{ring}$ ). The device fabrication starts with deep-UV lithography followed by photoresist reflow to reduce the line roughness. Waveguide etching is performed using C<sub>4</sub>F<sub>8</sub>/SF<sub>6</sub> based reactive ion etch assisted by a laser etch monitor for precise etch depth control. 620 nm thick PECVD SiO<sub>2</sub> is then deposited as the waveguide top cladding.

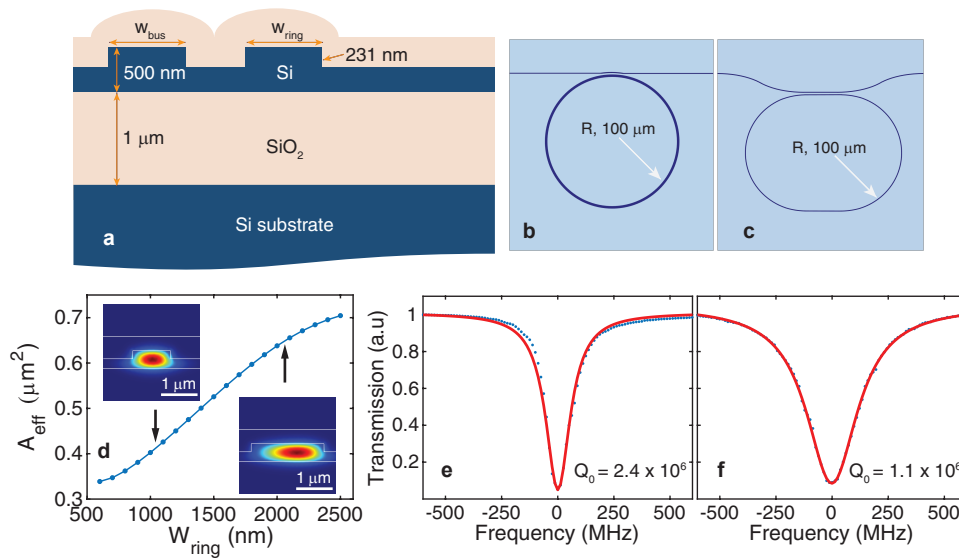


**Fig. 1.** (a) Schematics of cross section of the Si ring resonator at the bus-ring coupling region. (b), (c) Top-view schematics of the pulley-type ring and racetrack-type ring resonators. (d) Simulated effective mode area of the Si waveguide at 100  $\mu\text{m}$  bend radius. Insets show the simulated Si mode profile with two different ring waveguide width. (e) and (f) Fitted TE<sub>0</sub> mode resonance of pulley multimode ring resonator and racetrack quasi-single mode ring resonator. Measurements are in blue and Lorentzian fit is in red.

This set of ring resonators has 231 nm etch depth with an all-pass configuration and the top-view schematic is shown in Figs. 1(b) and 1(c). We can extract the Q-factor and power dependent loss from all-pass ring transmission measurement using the method described in the subsequent context. Two types of bus-ring waveguide couplers are used here, including pulley-type (Fig. 1(b)) and parallel waveguide racetrack-type (Fig. 1(c)), with 100  $\mu\text{m}$  ring radius. These two types of couplers have minimized coupler loss and all the straight to bend structures are made adiabatic to reduce the transition loss [24]. With optimized fabrication processes, these two types of resonator can result in high Q-factor and high intracavity power build up. For the pulley-type ring, the bus waveguide width is 960 nm and ring waveguide width is 2.06  $\mu\text{m}$ , which is multimode and support three transverse-electric mode (TE<sub>0</sub>, TE<sub>1</sub> and TE<sub>2</sub>). The racetrack-type ring has 1.07  $\mu\text{m}$  wide bus and ring waveguide. It is quasi-single mode at 100  $\mu\text{m}$  bend radius and only TE<sub>0</sub> mode is observed from the transmission spectrum. The simulated fundamental mode effective area as a function of  $W_{ring}$  with bend radius 100  $\mu\text{m}$  is plotted in Fig. 1(d). For a ring waveguide width of 2.06  $\mu\text{m}$  and 1.07  $\mu\text{m}$ , the effective mode area is  $\sim 0.65 \mu\text{m}^2$  and 0.42

$\mu\text{m}^2$ , respectively. The difference of the waveguide width results in different Q-factor as the mode overlaps with etched sidewall differently. One TE<sub>0</sub> mode resonance of each ring type is plotted in Fig. 1(e) and Fig. 1(f), for multimode pulley ring and quasi-single mode racetrack ring resonator, with fitted intrinsic Q-factor ( $Q_0$ ) is  $2.4 \times 10^6$  and  $1.1 \times 10^6$  respectively.

The Q-factor measurement above is performed with  $-17$  dBm power in the Si bus waveguide. The low power in the bus waveguide ensures the transmission spectrum is not distorted. This intrinsic Q-factor at low input power is referred to as 'cold-cavity'  $Q_{0c}$ . However, as the power build-up inside the ring resonator scales up with the ring Q-factor, high Q-factor also corresponds to high intracavity power intensity. We measured the power dependent transmission spectrum for the fabricated rings. The measurement is performed using an Agilent 81960A/81680A tunable laser and Agilent 81635A power sensor. The ring resonance is swept across from short wavelength to long wavelength for every sweep. A built-in wavemeter in the Agilent 8164B or Agilent 8163B Lightwave Multimeter corrects the absolute wavelength data during every sweep. Figure 2(a) shows the measurement results of a pulley type multimode ring with  $Q_{0c} = 1.7 \times 10^6$ . By increasing the input power during every sweep, the measured ring resonance red shifts as a function of the power in the bus waveguide, due to proportional index change from absorptive heating and Kerr nonlinearity as the intracavity power intensity increases. The shape of the resonator is Lorentzian at relatively low power levels, but the measurement becomes a non-Lorentzian, triangular shape at high power levels when the power in the bus waveguide is above  $-10$  dBm. This is due to the combined effect of the thermal refractive index-change and Kerr nonlinear index change as the laser scan wavelength is red detuned [25]. When the laser sweep wavelength increases across the effective resonance wavelength, the intracavity power will soon drop accompanied by resonance blue shift, and results in a quick increase in transmitted power to off-resonance state.

The resonator transmission is no longer Lorentzian shape, so the standard Lorentzian fitting is no longer applicable for the high-power levels. However, it is clearly shown in Fig. 2(a) that the minimum normalized transmission at resonance wavelength of every sweep keeps increasing when the sweep input power increases. Under a steady state where the coupler coupling strength is fixed, this indicates additional power is lost within the cavity system at high input power levels [26]. Similar to high-Q microdisk resonators, under all circumstances, the bus-ring waveguide cavity system can be described using three quality factors:  $Q_l$  (loaded Q),  $Q_0$  (intrinsic Q) and  $Q_c$  (coupler Q). They are related by  $1/Q_l = 1/Q_0 + 1/Q_c$ . At cold-cavity condition, this can be written as  $1/Q_{lc} = 1/Q_{0c} + 1/Q_{cc}$ . We can extract the  $Q_{lc}$ ,  $Q_{0c}$  and  $Q_{cc}$  at cold-cavity condition by Lorentzian fitting and the relation of  $Q_c = 2Q_l / (1 - \sqrt{T_{min}})$  and  $Q_0 = 2Q_c (1 - \sqrt{T_{min}}) / (1 + \sqrt{T_{min}})$  holds for all conditions with different power in the bus waveguide. At a steady state  $Q_c = Q_{cc}$  which is fixed, so it is convenient to extract the corresponding  $Q_0$  at different power levels. For this resonator, the cold-cavity finesse is about 650 and with 6.5 dBm bus waveguide power, the power intensity in the ring resonator is estimated to be around  $200 \text{ mW}/\mu\text{m}^2$ . The resonance shift is a combined effect of the thermal red shift and free carrier dispersion (FCD) blue shift. This FCD blue shift is determined by the free carrier density generated by TPA process in Si ring waveguide. Using equations describing the intensity dependent TPA process and FCA process, it shows the 23 pm resonance shift with 6.5 dBm bus waveguide results from the thermal red shift of  $\sim 46$  pm and FCD blue shift of  $\sim 23$  pm with FCD induced index change of  $-4.75 \times 10^{-5}$ . The free carrier density is about  $1.4 \times 10^{16} / \text{cm}^3$  if we assume a 23 ns free carrier lifetime and the temperature rise is calculated to be 0.5 K [27,28]. With this small temperature change, the coupler  $Q_c$  can be treated as a constant in the analysis. The derived thermal impedance is around 277 K/W. The total loss mainly consists of three parts, the linear loss ( $\alpha_l$ ), the TPA loss ( $\alpha_{TPA} = \beta_{TPA} \cdot I$ ), and FCA loss ( $\alpha_{FCA} = \sigma \cdot N_{FC}$ ), where  $I$  is the power intensity,  $\sigma$  is FCA cross section and  $N_{FC}$  is free carrier density.

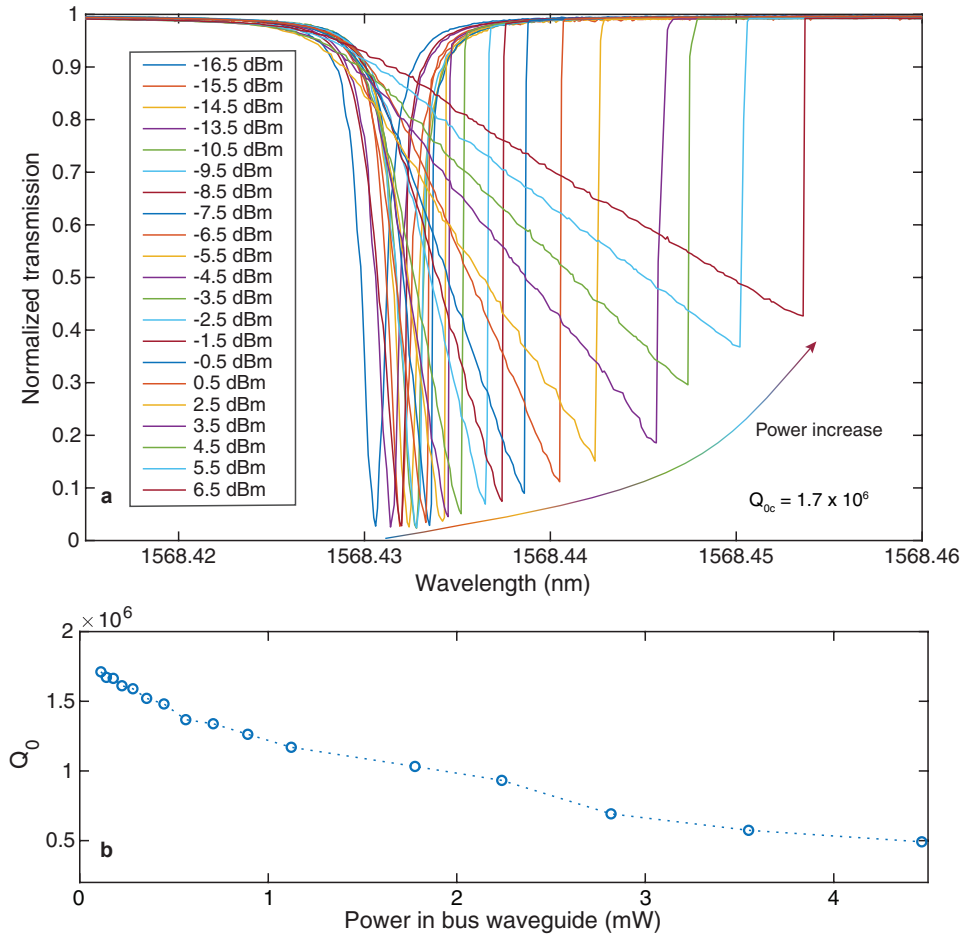


**Fig. 2.** (a) Normalized transmission at different bus waveguide power shown in the legend for a multimode pulley-ring Si resonator with  $Q_{0c} = 1.7 \times 10^6$ . (b) Extracted power dependent intrinsic Q-factor from (a).

The extracted intrinsic Q-factor with respect to different power levels shown in Fig. 2(a) is plotted in Fig. 2(b). The intrinsic Q-factor sees a clear drop with increased power in the bus waveguide.  $Q_0$  at 4.5 mW power in the bus waveguide drops to about  $0.5 \times 10^6$ , more than 3x reduction than its cold cavity  $Q_{0c}$ . The nonlinear loss will start to dominate at around 2.5 mW power in bus waveguide, when  $Q_0$  drops to half of  $Q_{0c}$ . This results from the high intracavity power build-up as a combined effect from high Q-factor and large free-spectral-range (FSR, 1.044 nm). Our conclusion still holds for an add-drop ring resonator, as the nonlinear loss depends on the similar intracavity power intensity. For a ring resonator used in tunable lasers, this large Q-factor drop will greatly deteriorate the laser performance, in terms of both output power and laser linewidth. More analysis will be discussed in Section 4.

### 3. Extended Si ring resonator and Si<sub>3</sub>N<sub>4</sub> ring resonator

For the use in a narrow-linewidth external cavity laser, a high-Q ring resonator needs to provide a long group delay, i.e. large effective cavity length for the reduction of modified Schawlow-Townes linewidth [29]. The passive/active section length ratio in a heterogeneously integrated external cavity laser plays an important role in determining the required ring resonator dimension. The effective length is determined by both power coupling strength ( $\kappa$ ) and physical radius  $R$  of the ring resonator:  $L_{eff} = 2\pi R(1 - \kappa)/\kappa$ . So, in addition to modifying the  $\kappa$ , an obvious method to increase the effective length is to simply increase the physical size of the ring resonator.

Here we fabricated another set of Si ring resonators with different etch depths and ring radii from the resonators in Section 2. The bus waveguide and ring waveguide now both have a width of 1.8  $\mu\text{m}$ . The etch depth is decreased to 56 nm and the ring radius is extended to 849  $\mu\text{m}$ , 711  $\mu\text{m}$  and 600  $\mu\text{m}$ , as illustrated in Figs. 3(a) and 3(b). For the three ring resonators sharing the same bus waveguide, the respective gap width between the waveguide and ring is tailored to keep a similar coupling coefficient. The transmission spectrum is taken by sweeping an Agilent 81608A tunable laser and recording the received voltage signal from an oscilloscope, after a fast photodetector. The measurement results are shown in Fig. 3(c). Figure 3(d) shows the separated resonance wavelength grouped by different FSRs corresponding to different ring radius.

Figure 3(e) shows the resonance transmission for each corresponding ring radius, with -7 dBm power in the bus waveguide. All these rings exhibit similar intrinsic Q-factor around  $0.75 \times 10^6$ , indicating no bending loss is limiting the total loss with radius over 600  $\mu\text{m}$ . The bottom row of each figure shows the normalized transmission at different power levels in bus waveguide from -7 dBm to 4 dBm. The frequencies are also aligned at each resonance to compare the relatively transmission. It can be seen, unlike the high-Q ring resonator transmission result in Fig. 2(a), these ring transmissions show quite similar profile at different power levels. Also, as the transmission minimum is not changed with the bus waveguide power, the power dependent Q-factor change is almost negligible.

This difference can be explained by three main reasons. First, due to the condition of etching equipment is not optimized in this process run, this set of resonators does not have Q-factor as high as  $4 \times 10^6$ , which is reported in our previous work [11]. Second, the extended ring radius would reduce the resonator finesse ( $\text{Finesse} = \lambda \cdot Q_l / (2\pi R \cdot n_g)$ ), together with the power build-up factor in the ring resonator proportionally. Third, the 1.8  $\mu\text{m}$  wide, 56 nm etch depth waveguide results in a large effective mode area of 0.91  $\mu\text{m}^2$ . So, the intracavity power density is reduced by the combined effects of reduced power build-up and large mode area. Compared with high-Q ring resonators in Section 2, this would lower the intracavity power density by an order of magnitude, even at same loaded Q-factor.

In heterogeneously integrated tunable lasers, other than extending the high-Q Si ring resonator to match the high-power application, another approach is to use a material system that is free of nonlinear loss at telecommunication wavelength band. Silicon nitride (Si<sub>3</sub>N<sub>4</sub>) is a complementary metal-oxide-semiconductor (CMOS) material that finds wide use in modern integrated circuit

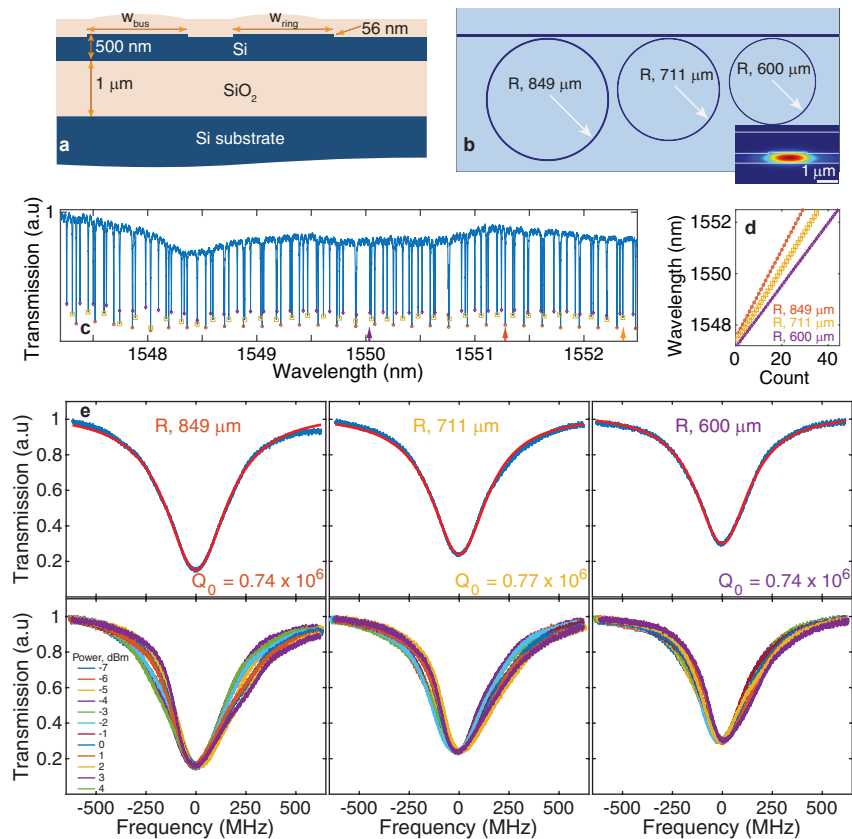


**Fig. 3.** (a) Schematics of cross-sectional view of the extended Si ring resonator at the bus-ring coupling region. (b) Top view schematics of three extended ring resonators sharing a common bus waveguide. Inset shows the simulated mode profile of Si extended ring with 849 μm radius. (c) Transmission measured from the common bus waveguide. (d) Resonance wavelength separated from (c), grouped by ring radius. (e) Fitted TE<sub>0</sub> mode resonance of extended ring resonators with difference ring radius. The bottom row shows normalized transmission aligned at corresponding resonance frequency for bus waveguide power ranging from -7 dBm to 4 dBm for each ring geometry.

(IC) technology. It has been used in heterogeneous integrated lasers with recent development in III-V/Si-Si<sub>3</sub>N<sub>4</sub> integration [23,30,31]. Also, hybrid integration of butt-coupled III-V gain material and Si<sub>3</sub>N<sub>4</sub> photonic circuits is another application field for Si<sub>3</sub>N<sub>4</sub> in a high-performance laser [32,33].

Here we measured the power dependent transmission properties of a fabricated Si<sub>3</sub>N<sub>4</sub> high-Q cavity with 1.6 mm ring radius. The cross section is shown in Fig. 4(a). The intrinsic Q-factor of the Si<sub>3</sub>N<sub>4</sub> ring resonator is  $8.3 \times 10^6$ , which corresponds to propagation loss of  $\sim 3.3$  dB/m (Fig. 4(b)). The effective mode area is around  $10 \mu\text{m}^2$ . Similar measurements of power dependent transmission sweeps as for extended Si rings are performed and the results are summarized in Fig. 4(c). The wavelength is shifted and normalized to each resonance wavelength respectively. It is clear at all power levels the normalized transmission almost shares the same minima. This measurement proves the power-dependent loss is negligible in Si<sub>3</sub>N<sub>4</sub>, even with very high Q-factor.

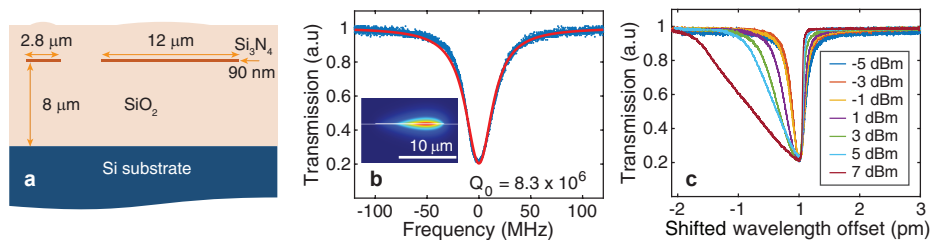


**Fig. 4.** (a) Schematics of cross-sectional view of Si<sub>3</sub>N<sub>4</sub> ring resonator at the bus-ring coupling region. (b) Fitted TE<sub>0</sub> mode resonance of Si<sub>3</sub>N<sub>4</sub> ring resonator top view schematics of three extended ring resonators sharing a common bus waveguide. Inset shows the simulated mode profile of Si<sub>3</sub>N<sub>4</sub> ring resonator. (c) Normalized transmission at different bus waveguide power shown in the legend for Si<sub>3</sub>N<sub>4</sub> ring resonator.

#### 4. Summary of the nonlinear loss effect

With the Q-factor extraction method described in Section 2, we can now summarize the power-dependent performance for all the resonators discussed above. The loss in the ring waveguide would be different from the loss in the bus waveguide because of nonlinear loss at high power intensity levels in the ring waveguide. Without considering the spatial loss modulation along the ring circumference, the extracted loss in the ring can be calculated from the ring resonator intrinsic Q-factor from  $\alpha = 2\pi n_g / Q_0 \lambda$ , where  $n_g$  is the group index and  $\lambda$  is the resonance wavelength.

The summarized power-dependent loss is shown in Fig. 5. A multimode Si ring with high Q-factor ( $2.4 \times 10^6$  and  $1.7 \times 10^6$ ) show lowest cold-cavity loss (0.3 and 0.4 dB/cm) among the Si resonators, but the extracted loss ramps up quickly when the bus waveguide power exceeds 0.5 mW, (around  $80 \text{ mW}/\mu\text{m}^2$  power density in the ring resonator). The loss become highest ( $> 1$  dB/cm) at bus waveguide power around 2 and 3 mW, respectively. A similar radius but smaller cross-section quasi-single-mode ring resonator with  $Q_{oc} = 1.1 \times 10^6$  also shows strong dependence with  $> 1$  mW bus waveguide power and the slope is similar to the  $1.7 \times 10^6$  multimode ring due to its smaller mode cross section resulting in similar power intensity despite the Q-factor difference. The extended Si ring resonator is quite power-independent as its loss is kept around 0.9 dB/cm, thanks to the relaxed intracavity power intensity. The Si<sub>3</sub>N<sub>4</sub> ring resonator shows negligible nonlinear loss, as expected.

Based on this analysis, for high-Q ( $> 1\text{M}$ ) Si resonator with small ring radius ( $\sim 100 \mu\text{m}$ ) and small cross section ( $\sim 0.4\text{-}0.7 \mu\text{m}^2$ ), the nonlinear loss becomes important at sub-mW bus

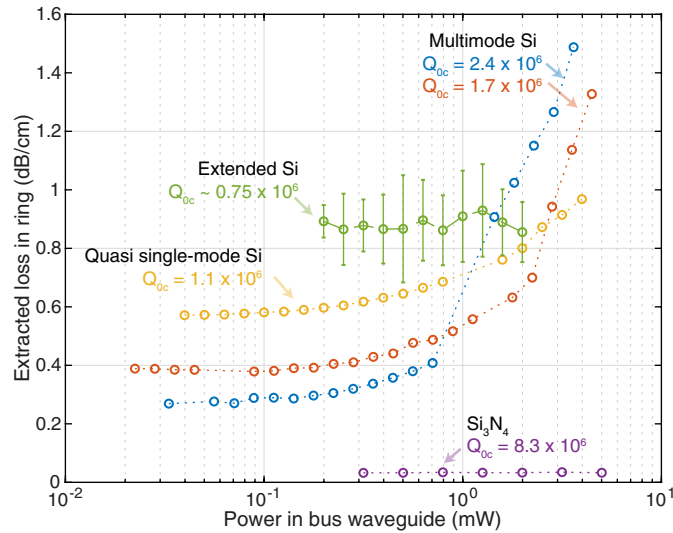


**Fig. 5.** Dependence of extracted loss in ring for different type of ring resonators on the power in bus waveguide.

waveguide power ( $< 100 \text{ mW}/\mu\text{m}^2$  power intensity in ring resonator) and dominates the overall loss of the laser system with only a few mW in the bus waveguide. It will scale up rapidly at higher power levels. They are thus not suitable for a high-performance narrow-linewidth laser, which normally works at this power range for many applications. This negative impact from nonlinear loss will limit the output power. And as the linewidth scales with  $1/P$ , the laser suffers from similar impairment on the linewidth performance at the same time. Further conclusions can be made that, even with arbitrary high gain material, the laser linewidth would not collapse in the end with this level of power-dependent loss and there would be a lower limit of the achievable linewidth, simply because of the nonlinear loss. Moreover, nonlinear absorption will also generate additional heat and increase the phase instability of the entire system. At moderate power levels, the existence of nonlinear self-pulsing and nonlinear hysteresis effects in an improperly designed high-Q Si ring resonator can further degrade the laser performance [17]. And once again, this detrimental effect will increase with an increased Q-factor and reduced ring resonator physical size (ring radius, ring waveguide cross section area, etc.).

To overcome this, one possible approach is to include a reverse biased p-i-n diode in the Si waveguide to avoid TPA-induced FCA [34]. This is widely used in Si Raman lasers to enable over 10x higher power handling capability for the Si waveguide. Using the TM mode in Si resonators could help reduce the confinement factor and lower the nonlinear absorption loss, however, this requires fabrication optimization to improve the TM mode Q-factor and decrease the linear loss. A more straightforward method is to design a high-Q ring resonator with reduced intracavity power density, i.e. extended Si ring resonator designs with large ring radius and large cross section. It has to be noted, due to the even smaller waveguide core size of 220 nm thick Si waveguides in a standard silicon photonics foundry, this power dependent loss would be a more important limiting factor in getting a high power, narrow-linewidth butt-coupled Si laser. Beyond this, we anticipate, due to the ultra-low loss of  $\text{Si}_3\text{N}_4$  waveguides and their negligible nonlinear loss, ring-resonator based III-V/Si/ $\text{Si}_3\text{N}_4$  widely tunable heterogeneously integrated lasers should achieve unprecedented laser performance. Another promising platform for heterogeneous lasers

is AlGaAs-on-insulator. While it can enable waveguides with loss comparable to Si, its bandgap can be tailored by altering the Al content to avoid TPA at telecom wavelengths to minimize nonlinear loss [35]. Together with its high nonlinearity, this could enable a new class of devices.

## 5. Conclusion

We experimentally characterized the nonlinear loss in different types of high-Q Si ring resonators. The nonlinear loss in high-Q Si ring resonators dominates the total loss at power levels where a typical heterogeneously integrated laser would work (a few mW). The benefits of using extended Si ring resonators and Si<sub>3</sub>N<sub>4</sub> ring resonators are compared and analyzed. Our results provide important conclusions that must be addressed with refined high-Q ring resonator designs in heterogeneously integrated and butt-coupled III-V/Si laser systems to achieve even narrower linewidths than the 120 Hz Lorentzian linewidth demonstrated to date.

## Funding

Defense Advanced Research Projects Agency (DARPA) (HR0011-15-C-055, W911NF-19-C-0003).

## Acknowledgements

The authors thank Minh Tran for helpful discussions and Jonathan Peters for sample preparation.

## Disclosures

The authors declare no conflicts of interest.

## References

1. R. Jones, P. Doussiere, J. B. Driscoll, W. Lin, H. Yu, Y. Akulova, T. Komljenovic, and J. E. Bowers, "Heterogeneously Integrated InP/Silicon Photonics: Fabricating Fully Functional Transceivers," *IEEE Nanotechnol. Mag.* **13**(2), 17–26 (2019).
2. K. Zou, Z. Zhang, P. Liao, H. Wang, Y. Cao, A. Almainan, A. Fallahpour, F. Alishahi, N. Satyan, G. Rakuljic, M. Tur, A. Yariv, and A. Willner, "Higher-order QAM Data Transmission Using a High-Coherence Hybrid Si/III-V Semiconductor Laser," *Opt. Lett.* **45**(6), 1499–1502 (2020).
3. W. Xie, T. Komljenovic, J. Huang, M. Tran, M. Davenport, A. Torres, P. Pintus, and J. Bowers, "Heterogeneous silicon photonics sensing for autonomous cars [Invited]," *Opt. Express* **27**(3), 3642 (2019).
4. G. M. Brodnik, M. W. Harrington, D. Bose, A. M. Netherton, W. Zhang, L. Stern, P. A. Morton, J. E. Bowers, S. B. Papp, and D. J. Blumenthal, "Chip-Scale, Optical-Frequency-Stabilized PLL for DSP-Free, Low-Power Coherent QAM in the DCI," in *Optical Fiber Communication Conference (OFC) 2020* (OSA, 2020), p. M3A.6.
5. E. Dale, W. Liang, D. Eliyahu, A. A. Savchenkov, V. S. Ilchenko, A. B. Matsko, D. Seidel, and L. Maleki, "Ultra-narrow line tunable semiconductor lasers for coherent LIDAR applications," in *Imaging and Applied Optics 2014, OSA* (Optical Society of American (OSA), 2014), p. JTu2C.3.
6. C. T. Santis, Y. Vilenchik, N. Satyan, G. Rakuljic, and A. Yariv, "Quantum control of phase fluctuations in semiconductor lasers," *Proc. Natl. Acad. Sci. U. S. A.* **115**(34), E7896–E7904 (2018).
7. D. Huang, M. A. Tran, J. Guo, J. Peters, T. Komljenovic, A. Malik, P. A. Morton, and J. E. Bowers, "High-power sub-kHz linewidth lasers fully integrated on silicon," *Optica* **6**(6), 745 (2019).
8. M. A. Tran, D. Huang, J. Guo, T. Komljenovic, P. A. Morton, and J. E. Bowers, "Ring-Resonator Based Widely-Tunable Narrow-Linewidth Si/InP Integrated Lasers," *IEEE J. Sel. Top. Quantum Electron.* **26**(2), 1–14 (2020).
9. M. A. Tran, D. Huang, and J. E. Bowers, "Tutorial on narrow linewidth tunable semiconductor lasers using Si/III-V heterogeneous integration," *APL Photonics* **4**(11), 111101 (2019).
10. C. T. Santis, S. T. Steger, Y. Vilenchik, A. Vasilyev, and A. Yariv, "High-coherence semiconductor lasers based on integral high-Q resonators in hybrid Si/III-V platforms," *Proc. Natl. Acad. Sci. U. S. A.* **111**(8), 2879–2884 (2014).
11. M. Tran, D. Huang, T. Komljenovic, J. Peters, A. Malik, and J. Bowers, "Ultra-Low-Loss Silicon Waveguides for Heterogeneously Integrated Silicon/III-V Photonics," *Appl. Sci.* **8**(7), 1139 (2018).
12. L. A. Coldren, S. W. Corzine, and M. L. Mašanović, *Diode Lasers and Photonic Integrated Circuits* (John Wiley & Sons, Inc., 2012).
13. J. Heebner, R. Grover, and T. Ibrahim, "Optical microresonator theory," *Springer Ser. Opt. Sci.* **138**, 71–103 (2008).
14. W. Bogaerts, P. De Heyn, T. Van Vaerenbergh, K. De Vos, S. Kumar Selvaraja, T. Claes, P. Dumon, P. Bienstman, D. Van Thourhout, and R. Baets, "Silicon microring resonators," *Laser Photonics Rev.* **6**(1), 47–73 (2012).

15. Q. Lin, O. J. Painter, and G. P. Agrawal, "Nonlinear optical phenomena in silicon waveguides: modeling and applications," *Opt. Express* **15**(25), 16604 (2007).
16. Y. Guo, W. Zhang, N. Lv, Q. Zhou, Y. Huang, and J. Peng, "The impact of nonlinear losses in the silicon micro-ring cavities on CW pumping correlated photon pair generation," *Opt. Express* **22**(3), 2620 (2014).
17. T. J. Johnson, M. Borselli, and O. Painter, "Self-induced optical modulation of the transmission through a high-Q silicon microdisk resonator," *Opt. Express* **14**(2), 817 (2006).
18. X. Sun, X. Zhang, C. Schuck, and H. X. Tang, "Nonlinear optical effects of ultrahigh-Q silicon photonic nanocavities immersed in superfluid helium," *Sci. Rep.* **3**(1), 1436 (2013).
19. A. Misra, S. Preußler, L. Zhou, and T. Schneider, "Nonlinearity- and dispersion- less integrated optical time magnifier based on a high-Q SiN microring resonator," *Sci. Rep.* **9**(1), 1–11 (2019).
20. P. Morton and J. Khurgin, "Low noise, high power, multiple microresonator based laser," U.S. Patent 9, 559, 484, Jan. 31, 2017.
21. P. Morton, J. Khurgin, and C. Morton, "Multiple-microresonator based laser," U.S. Patent 9748726, Aug. 29, 2017.
22. C. Xiang, P. A. Morton, J. Khurgin, C. Morton, and J. E. Bowers, "Widely tunable Si<sub>3</sub>N<sub>4</sub> triple-ring and quad-ring resonator laser reflectors and filters," in *Proc. IEEE 15th Int. Conf. Group IV Photon.*, 2018, pp. 1–2.
23. C. Xiang, W. Jin, J. Guo, J. D. Peters, M. J. Kennedy, J. Selvidge, P. A. Morton, and J. E. Bowers, "Narrow-linewidth III-V/Si<sub>3</sub>N<sub>4</sub> laser using multilayer heterogeneous integration," *Optica* **7**(1), 20 (2020).
24. C. Xiang, M. L. Davenport, J. B. Khurgin, P. A. Morton, and J. E. Bowers, "Low-Loss Continuously Tunable Optical True Time Delay Based on Si<sub>3</sub>N<sub>4</sub> Ring Resonators," *IEEE J. Sel. Top. Quantum Electron.* **24**(4), 1–9 (2018).
25. T. Carmon, L. Yang, and K. J. Vahala, "Dynamical thermal behavior and thermal self-stability of microcavities," *Opt. Express* **12**(20), 4742–4750 (2004).
26. M. Borselli, T. J. Johnson, and O. Painter, "Beyond the Rayleigh scattering limit in high-Q silicon microdisks: theory and experiment," *Opt. Express* **13**(5), 1515 (2005).
27. H. Rong, A. Liu, R. Nicolaescu, M. Paniccia, O. Cohen, and D. Hak, "Raman gain and nonlinear optical absorption measurements in a low-loss silicon waveguide," *Appl. Phys. Lett.* **85**(12), 2196–2198 (2004).
28. J. Leuthold, C. Koos, and W. Freude, "Nonlinear silicon photonics," *Nat. Photonics* **4**(8), 535–544 (2010).
29. R. Kazarinov and C. Henry, "The relation of line narrowing and chirp reduction resulting from the coupling of a semiconductor laser to passive resonator," *IEEE J. Quantum Electron.* **23**(9), 1401–1409 (1987).
30. J. F. Bauters, M. L. Davenport, M. J. R. Heck, J. K. Doyle, A. Chen, A. W. Fang, and J. E. Bowers, "Silicon on ultra-low-loss waveguide photonic integration platform," *Opt. Express* **21**(1), 544 (2013).
31. M. Piels, J. F. Bauters, M. L. Davenport, M. J. R. Heck, and J. E. Bowers, "Low-loss silicon nitride AWG demultiplexer heterogeneously integrated with hybrid III-V/Silicon photodetectors," *J. Lightwave Technol.* **32**(4), 817–823 (2014).
32. C. Xiang, P. A. Morton, and J. E. Bowers, "Ultra-narrow linewidth laser based on a semiconductor gain chip and extended Si<sub>3</sub>N<sub>4</sub> Bragg grating," *Opt. Lett.* **44**(15), 3825 (2019).
33. K.-J. Boller, A. van Rees, Y. Fan, J. Mak, R. E. M. Lammerink, C. A. A. Franken, P. J. M. van der Slot, D. A. I. Marpaung, C. Fallnich, J. P. Epping, R. M. Oldenbeuving, D. Geskus, R. Dekker, I. Visscher, R. Grootjans, C. G. H. Roeloffzen, M. Hoekman, E. J. Klein, A. Leinse, and R. G. Heideman, "Hybrid Integrated Semiconductor Lasers with Silicon Nitride Feedback Circuits," *Photonics* **7**(1), 4 (2020).
34. H. Rong, R. Jones, A. Liu, O. Cohen, D. Hak, A. Fang, and M. Paniccia, "A continuous-wave Raman silicon laser," *Nature* **433**(7027), 725–728 (2005).
35. L. Chang, A. Boes, P. Pintus, W. Xie, J. D. Peters, M. J. Kennedy, W. Jin, X.-W. Guo, S.-P. Yu, S. B. Papp, and J. E. Bowers, "Low loss (Al)GaAs on an insulator waveguide platform," *Opt. Lett.* **44**(16), 4075 (2019).